Study of the Discharge Chamber Magnetic Field Configuration Effects on the Electron Cyclotron Resonance (ECR) Microwave Ion Thruster

Yavuz Emre Kamis* and Murat Celik†

Bogazici University, Istanbul, 34342, Turkey

Abstract

Microwave ion thrusters that employ the gyromotion of the electrons around an external static magnetic field lines to obtain discharge are among the most selected devices for deep space missions that require longer life time. The phenomenon of electron cyclotron resonance (ECR) is utilized to a high degree to energize the electrons in magnetic tubes created by the lines of force and obtain discharge through impact ionization. A discussion for the trade-offs between microwave systems to other electric propulsion systems is presented along with numerical simulations on some designs from literature. COMSOL Multiphysics, a finite element software, is used to conduct magnetic field simulation, electromagnetic simulation and plasma simulation. Results show that the increase in number of magnets and orienting them to form cusps affect the density and temperature distribution by increasing the magnetic tubes in which the electrons are trapped and energized. The R-mode and X-mode resonance regions are plotted, and for 20mN-class ion thruster it is verified that X-mode resonance is the dominant energy transfer mechanism.

I.   Introduction

AFTER DC and RF technologies were well studied and put into practice, both as thrusters and neutralizers, a need for a third way of electric propulsion has emerged. Due to lifetime limitations of the first two, deep space missions were not feasible. Microwave discharge ion thrusters and neutralizers were considered to be a third electric propulsion system, for its less complicated structure compared to DC and RF devices, and electrodeless or rather emitterless nature that extends the lifetime substantially, since the plasma cathode body acts as a positively biased electrode, collecting ion current from the thruster plume.[1] Microwave thrusters use the gyromotion of electrons around external static magnetic field lines to obtain a discharge. The cyclotron frequency of an electron is given by

$$\omega_c = \frac{eB}{m_e} \tag{1}$$

where e is the elementary charge, B is the applied magnetic field flux density and m_e is the mass of an electron. When this frequency is matched to that of the microwave, the microwave energy is resonantly absorbed by the electrons and impact ionization of the propellant atoms is achieved.

The μ10 neutralizer on HAYABUSA has delivered 140 mA of beam current when operating with 0.5 sccm xenon gas flow with a discharge voltage of -48 V, relative to the space potential of the ion beam. Absorbed microwave power by the neutralizer was 8 W at 4.2 GHz, whose schematic is shown in Figure 1. The total electron production cost in terms of the power consumption is 105 W/A, taking the microwave power and the beam extraction power into account.

---

*Graduate Student, Mechanical Engineering, Bogazici University.
†Assistant Professor, Mechanical Engineering, Bogazici University.

American Institute of Aeronautics and Astronautics

Another ECR plasma cathode that was used as a neutralizer was demonstrated in.[2] This cathode which was studied at the University of Michigan in Ann Arbor, was investigated in terms of discharge and electron extraction properties. The maximum electron current can be extracted was on the order of 0.6 A, for an argon gas flow rate of 5.6 sccm, with a discharge voltage difference of 40 V and 200 W of microwave power.
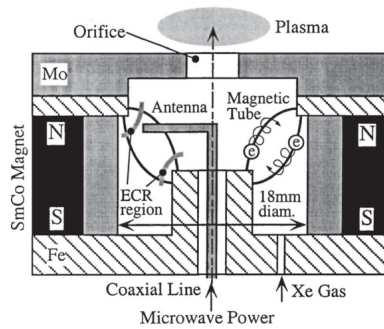

Figure 1. 4.2 GHz neutralizer cathode[3] of $\mu10$ ion thruster

NASA's ECR cathode which had been considered as a neutralizer for the High Power Electric Propulsion (HiPEP) thruster was excited at a lower frequency, 2.45 GHz; at a xenon gas flow rate of 3.5 sccm and delivered microwave power of 125 W, extractable electron current was on the order of 2.45 A at a bias voltage of 70 V.[4] NASA's Evolutionary Xenon Thruster (NEXT) which uses a hollow cathode assembly as a neutralizing device, has a 10 W/A electron production cost.[5] One can conclude that the cost of extracting electrons in ECR is significantly higher than that of hollow cathode. The difference is mainly because of the confinement of electrons in the ECR zone. Though this provides a much higher plasma density than hollow cathodes, the strong magnetic field also obstructs the diffusion of the electrons from the ECR region, thus making it harder to extract electron current. The trade off is such that ECR neutralizers are much less-energy efficient but have a much longer lifetime when compared to hollow cathodes as they do not have emitters which strongly limit the lifetime of the device.[1] Therefore, it serves as a key design parameter that the confinement of the electrons by the static magnetic field must be optimized such that the power consumed to extract electrons from the ECR zone must not be substantial.

The Hayabusa spacecraft that utilized $\mu10$ microwave ion thruster for the asteroid mission described in,[7] was improved further as a 20cm diameter thruster, $\mu20$, whose operational characteristics were presented in.[8] The 20 cm thruster had a 500 mA of ion beam current with a production cost of 200 W/A. 100 W of microwave power was supplied to the ion source antenna. While the $\mu10$ ion thruster had developed an average thrust of 8 mN, the $\mu20$ thruster operates with an average thrust of 27 mN, which is mainly caused by the enlargement of the discharge chamber. The neutralizer for the $\mu20$ thruster was designed to be the same as $\mu10$'s, with higher gas flow rate and microwave power in order to extract the necessary electron current which is on the order of 500 mA.[8]

The designs for the 20 mN-class and $\mu20$ ion thrusters presented in[6] and[9] respectively, are numerically investigated in this paper. On the 20mN-class ion thruster, microwave is fed to the discharge chamber via a coaxial antenna through an aluminum circular waveguide at 4.2 GHz frequency. Inside the discharge chamber, two Samarium Cobalt ring magnets were mounted on an iron yoke plate.[6] The $\mu20$ thruster, on the other hand, has four concentric ring magnets and microwave is fed directly by a coaxial antenna into the discharge chamber.[9]

II.   Theory

To get a deeper understanding of the ECR phenomenon, electromagnetic wave propagation in plasma must be studied. Dispersion relation for electromagnetic waves inside magnetized plasma is in tensor form, because the oscillating electric field will result in a current not in the same direction with itself, due to $\mathbf{E} \times \mathbf{B}$ drift. For propagation along the external magnetic field ($\mathbf{k} \parallel \mathbf{B_s}$) and propagation perpendicular to the external magnetic field ($\mathbf{k} \perp \mathbf{B_s}$), cut off and resonance behaviors show differences.

For the case of parallel propagation, the solution of the tensor dispersion relation obtained from Maxwell's equations will yield two roots, right circularly polarized solution (i.e. $E_y = iE_x$), also known as R-mode
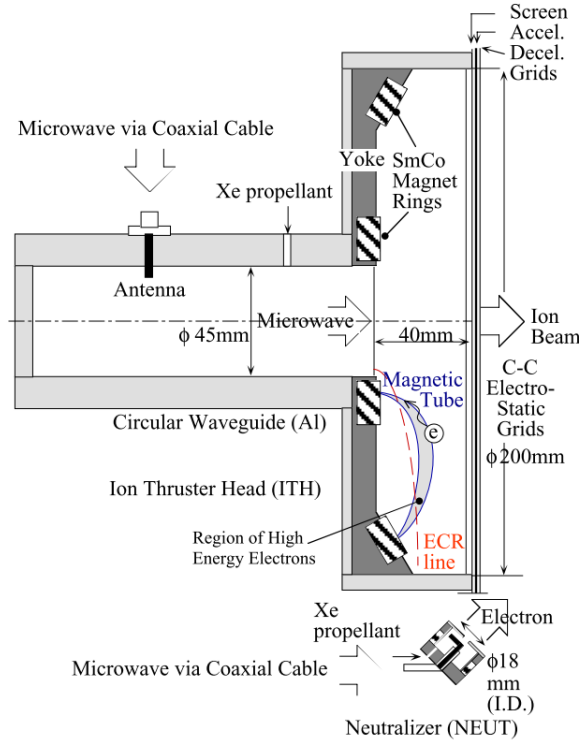
Figure 2. Schematic of the thruster head and the circular waveguide of the 20mN-class microwave ion thruster[6]

or left circularly polarized solution (i.e. $E_y = -iE_x$), also known as L-mode. When collisions and ion contributions are neglected, Equation 2 describes the right handed dispersion relation.

$$k = \frac{\omega}{c}\left[1 - \frac{\omega_p^2}{\omega(\omega - \omega_c)}\right]^{1/2} \tag{2}$$

where k is the wavenumber, c is the speed of light, ω_p is the plasma frequency, ω_c is the cyclotron frequency and ω is the microwave frequency.

So for a fixed microwave frequency, there is a corresponding cyclotron frequency or magnetic field, that makes the wave number diverge and makes the gyromotion of the electron and the electromagnetic wave in phase, allowing an unbounded acceleration of electrons. In order for the wave number to diverge and be real valued, $\omega = \omega_c$ has to be satisfied as well as $\omega_c \to \omega^+$. That means the wave has to be launched along a decreasing magnetic field. The cutoff condition for the R-mode, which needs to be addressed when the propagation properties of the wave inside a cold plasma is discussed, can be found by setting the left hand side of Equation 2 to zero.

$$\omega_R = \frac{1}{2}[\omega_c + \sqrt{\omega_c^2 + 4\omega_p^2}] \tag{3}$$

For the case of perpendicular propagation, the two possible solutions become the Ordinary mode (O-mode) where the oscillation of the electric field is parallel to the external magnetic field so the magnetic field has no effect on wave propagation; and Extraordinary mode (X-mode) where the oscillation of the electric field, the wave propagation and the external magnetic field are all perpendicular to each other. The dispersion relation for X-mode gets the form in Equation 4 which will have a resonance when $\epsilon_{xx} = 0$.

$$k^2 = \frac{\omega^2}{c^2}\frac{\epsilon_{xx}^2 + \epsilon_{xy}^2}{\epsilon_{xx}} \tag{4}$$

where ϵ represents the plasma permittivity tensor and the subscripts are the associated directional components.

American Institute of Aeronautics and Astronautics

This equation yields two resonance conditions, that will respectively be called upper hybrid and lower hybrid frequencies. For high frequency waves such as microwaves, lower hybrid resonance is neglected, the expression for upper hybrid resonance frequency is
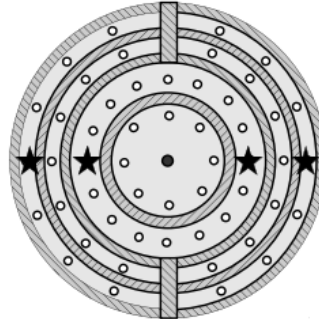
$$\omega_{UH}^2 = \omega_c^2 + \omega_p^2 \tag{5}$$

Figure 3. Schematic of the μ20 ion thruster[9]

III. Numerical Method

The schematics of the thrusters studied in this paper are shown in Figures 2 and 3. Figure 2 shows the circular waveguide and thruster head region of the 20mN-class ion thruster. In Figure 3, downstream view of the thruster is shown, where stars represent the gas inlets and the dot at the center represents the microwave antenna. The numerical simulations was developed using COMSOL, a finite element software. The modeling had three stages, first the magnetic field simulation was conducted. The static magnetic field topology caused by the Samarium Cobalt ring magnets and affected by the iron yoke plate was simulated both in 3D and 2D-axisymmetric domains. Then the electromagnetic simulation was conducted in 3D, since the coaxial cable violates axisymmetry. Figure 4 shows the 3D domain of the 20mN-class ion thruster design of.[6]
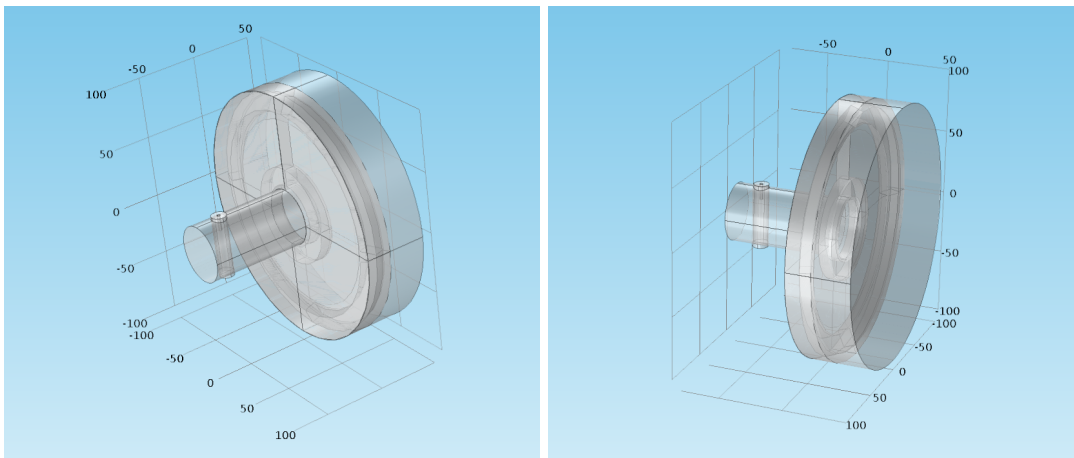

Figure 4. 3D computational domain of the 20mN-class microwave ion thruster shown at different angles

After the magnetic field simulation is completed, mesh is refined in order to redistribute the computational cost so that a finer mesh is obtained near the ECR region. The solution of the magnetic field simulation is fed back into the model using Equation 6 to create the new mesh.

$$N_{element}(|\mathbf{B}|) = \frac{1}{||\mathbf{B}| - 0.15| + \varepsilon} \tag{6}$$

American Institute of Aeronautics and Astronautics

where 0.15 T is the corresponding critical magnetic field for 4.2 GHz and ε is an arbitrary small number to prevent division by zero. The refined mesh is further improved by the addition of boundary layers at the walls to account for sheath formation where there is a voltage and density gradient across few Debye lengths. The final mesh in 2D-axisymmetric domain, shown in Figure 5, is used for plasma simulation, which is the third stage of the modeling. For the electromagnetic simulation, frequency-domain solver was used to
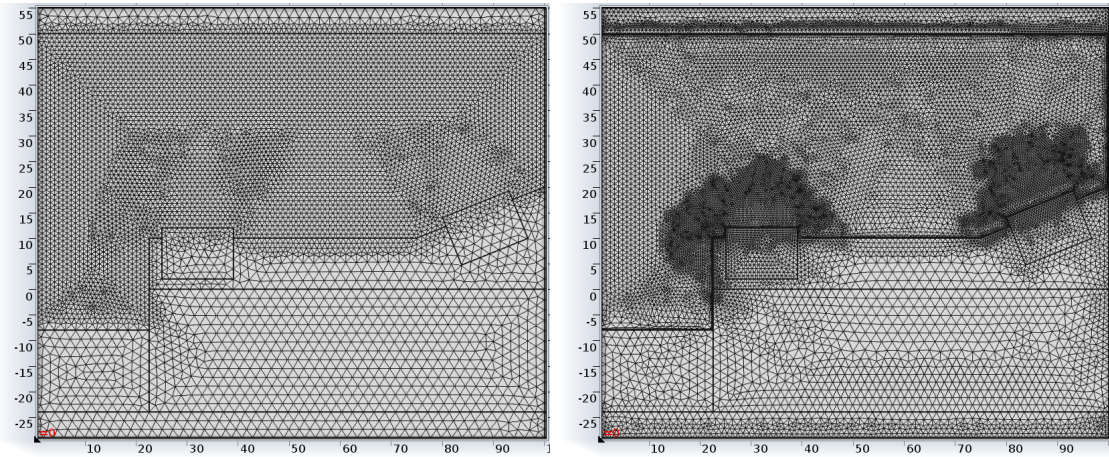

Figure 5. Initial (left) and refined (right) mesh of the 2D-axisymmetric domain of the 20mN-class ion thruster

solve the model at 4.2 GHz frequency. 90 W microwave power was fed from the coaxial antenna and guided through an aluminum circular waveguide with 45 mm diameter in TE_{11} mode.

IV. Results

The magnetic field simulation, the electromagnetic simulation and the plasma simulation were solved successively. The solutions were used as boundary conditions or background fields to solve for the plasma properties.

A. Magnetic Field Simulation

For two different configurations, magnetic field topologies were solved. The iron yoke plates that the ring SmCo magnets are mounted on, act as a guide to collect the field lines because of their high relative permeability. The field lines in the axisymmetric domain are plotted as the contours of the out-of-plane component of the vector potential. Formation of the mirror field and magnetic tubes can be seen in Figure 6. The narrow region around the critical magnetic field, with magnitude of 0.15 T, is shown with red.
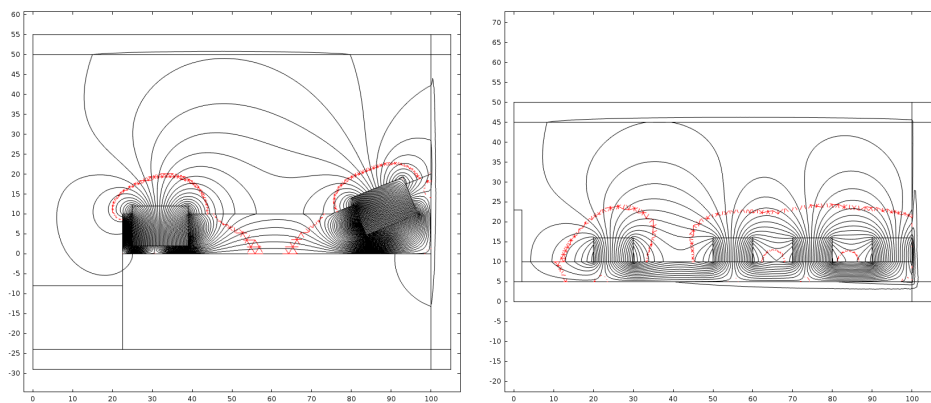

Figure 6. Magnetic field topologies and the ECR lines (shown in red) of 20mN-class (left) and μ20 (right) ion thrusters

American Institute of Aeronautics and Astronautics

B.   Electromagnetic Simulation

For the 20mN-class ion thruster, the configuration includes a coaxial antenna-waveguide coupling which is solved in the electromagnetic simulation. 90 W excitation was placed as a port boundary condition at the coaxial antenna where the second port was the end of the waveguide without any excitation. To verify the simulation, a transverse cross-section of the circular waveguide was taken and the electric field arrows were plotted, as shown in Figure 7. As can be seen from this figure, the electric field lines agree with the expected topology of TE_{11} mode.
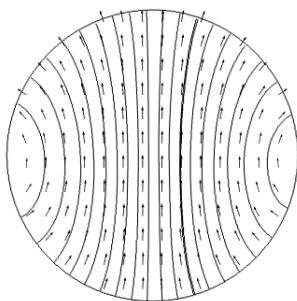

Figure 7.   The electric field solution inside the waveguide: the topology agrees with TE_{11} mode

Slice plots on the 3D domain were chosen to visualize the electric field norm around the coaxial antenna, inside the waveguide and near the grids as shown in Figure 8. The electric field distribution inside the discharge chamber is essential for accounting the heating in the ECR region because perpendicular component of the electric field to the static magnetic field is to be maximized in order to increase the energy absorption by the electrons inside the ECR region according to Equation 7.[10]

$$\mathcal{E}_{ECR} = \pi e \frac{E_\perp^2}{v_\parallel \left| \frac{\partial \mathbf{B}}{\partial s} \right|} \tag{7}$$

where $\left| \frac{\partial \mathbf{B}}{\partial s} \right|$ is the gradient of magnetic flux along a field line, $E_\perp$, is the component of the electric field that is perpendicular to the external magnetic field lines and $v_\parallel$ is the velocity of the electrons parallel to the external magnetic field lines. The time-averaged power flow of the microwave inside the 20mN-class ion thruster head and the electric field norm is shown in Figure 8.
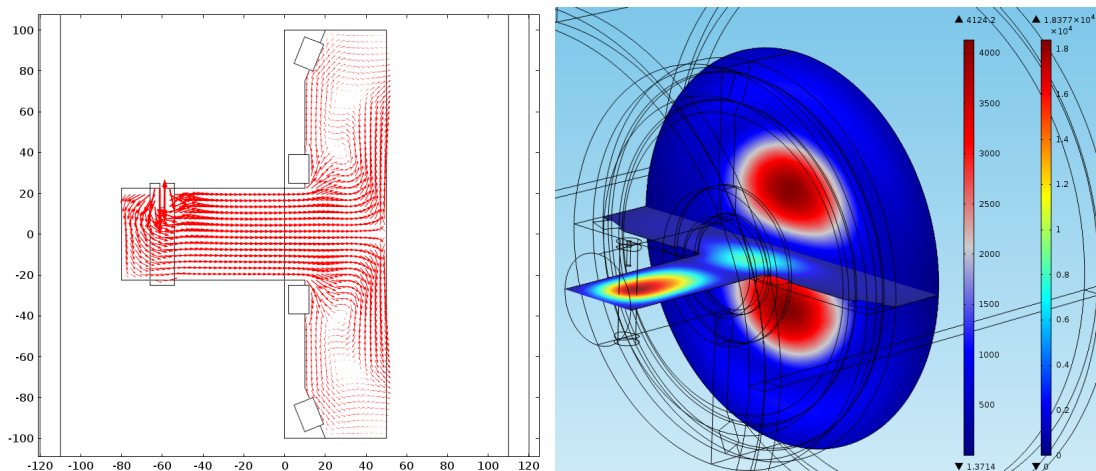

Figure 8.   The arrow plot of the microwave time-averaged power flow (left) and the associated electric field magnitude distribution inside the waveguide and discharge chamber (right)

American Institute of Aeronautics and Astronautics

C.   Plasma Simulation

The solutions from the magnetic field simulations were used as the background magnetic field in the plasma module for both of the analyzed devices. To lower the computational cost, discharge chamber was modeled as 2D-axisymmetric. The violation of the axisymmetry by the coaxial antenna was overcome by including only a small portion of the waveguide upstream of the antenna where the axisymmetry is not violated. The electric field distribution at the entrance of the included portion of the waveguide was taken from the 3D electromagnetic simulation and those solutions were implemented as the port excitation in the 2D simulation. Argon was the propellant of choice in both of the models. Xenon has a lower ionization energy than argon so the simulations conducted with argon are expected to have slightly lower densities than the results obtained with xenon in the literature. The collision cross section data were implemented from the library of COMSOL. To ensure that 90 W of power is absorbed by the electrons, the volume integral of the inductive heating term, P_{ind}, is scaled by a factor α as shown in Equation 8, similar to the technique described in.[11]

$$\alpha = \frac{90W}{\int \int \int P_{ind} dV} \tag{8}$$

The solutions of density distributions for 20mN-class and μ20 thrusters are compared in Figure 9. The peak in the density distribution of 20mN-class thruster in the magnetic tube formed by the field lines is in agreement with.[3]
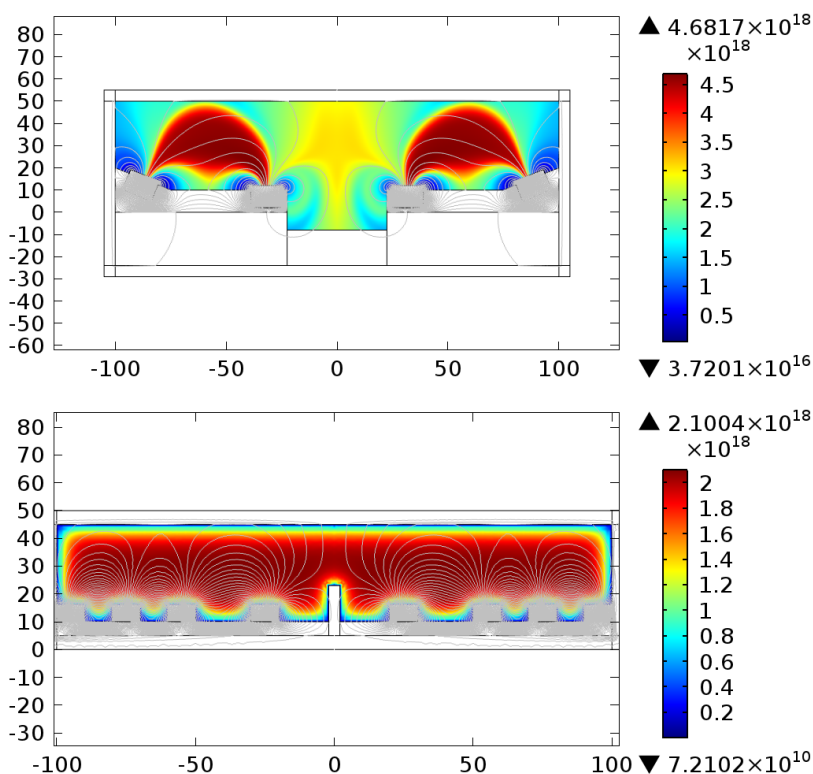

Figure 9. The electron density distributions in m^{-3} of 20mN-class (top) and μ20 (bottom) ion thrusters, with the magnetic field lines shown in gray contours

One of the reasons of the uniformity of the plasma density in μ20 is the increase in the number of magnets which causes an enhanced area of energized electrons that cause impact ionization. Another reason might be the means of microwave transmission as in μ20, the microwave is carried by a coaxial cable whose antenna is placed directly inside the discharge chamber. The antenna being closer to the ECR region increases the effective plasma production.[12] Also looking at the electron density distribution of μ20 ion thruster, the electron density can be observed to fall significantly near the walls of the discharge chamber, verifying the sheath formation.

The plots of electron temperature distribution shown in Figure 10 reveal that magnetic tubes form regions of high temperature electrons. This agrees with theory, as mirror confinement of the electrons energize them inside the tube regions causing a significant increase in electron thermal energy.
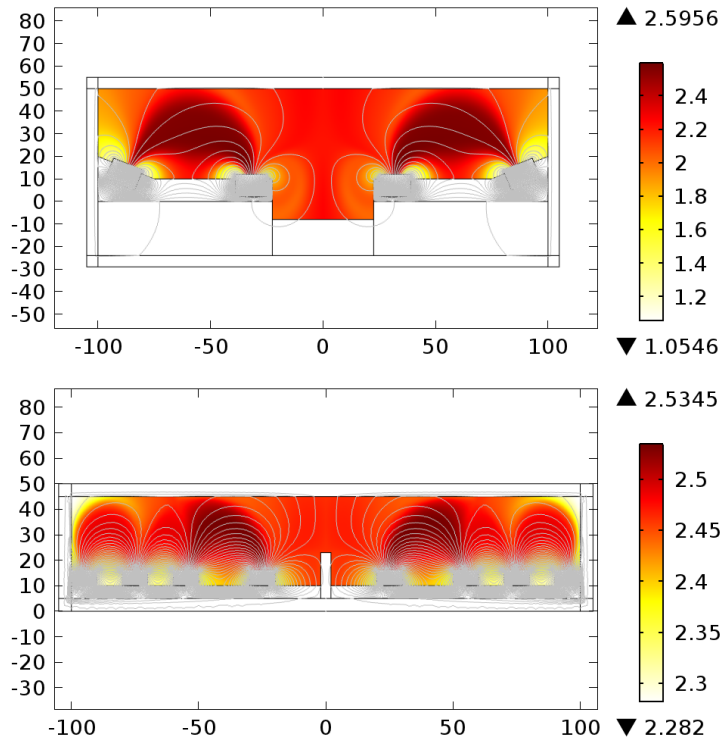

Figure 10. Electron temperature distributions in eV of 20mN-class (top) and μ20 (bottom) ion thrusters

The solutions may also be used to investigate and verify the mode competitions of the wave propagation inside the plasma. In the 20mN-class ion thruster, since the waves reach the resonance zone perpendicular to the magnetic field, X-mode resonance is suggested to be the dominant energy transfer mechanism.[6] Figure 11 verifies this suggestion, the resonance zones of R-mode and X-mode are shown in red and black lines respectively, and the power dissipation plot presented on the right in the same figure shows that at upper hybrid resonance regions, the power dissipation increases. An increase in the power dissipation is also visible in the regions where X-mode resonance zones and R-mode resonance zones overlap.
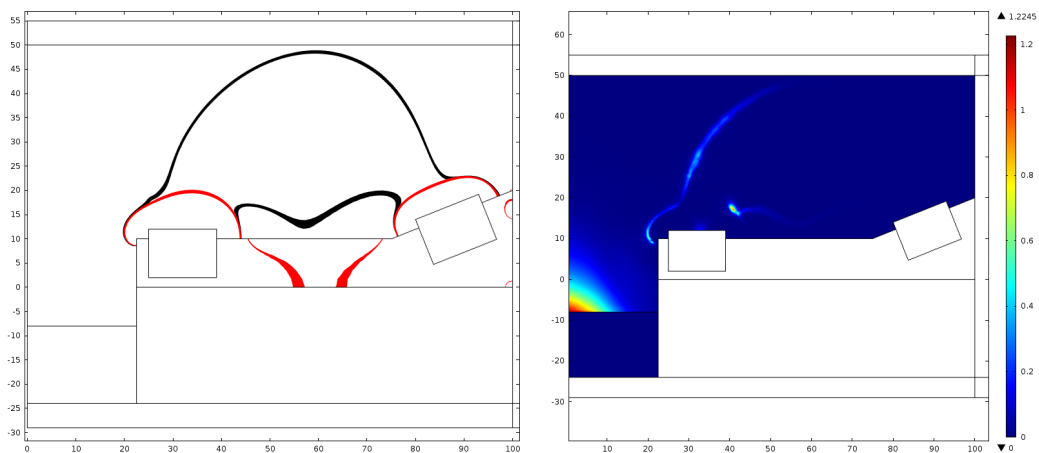

Figure 11. The R-mode (red) and X-mode (black) resonance regions (left) and the surface plot for power dissipation density in W/cm^3 (right) of 20 mN-class ion thruster

American Institute of Aeronautics and Astronautics

In microwave ion thrusters, the delivered microwave power is limited because a plasma density that would exceed the cut off density would result in the microwaves to be reflected, thus not delivering power to the resonance region. On the other hand, it is suggested that the small geometry of the discharge chamber would allow the R-mode waves to partially propagate through the region between right handed cutoff and ECR lines.[3]

V.   Conclusion

The 20 mN-class ion thruster and μ20 ion thruster were investigated numerically, using COMSOL Multiphysics, a finite element software. The magnetic field topologies were plotted and their effects on plasma simulation results were visualized and discussed. Results show the the density distribution is highly affected by the strength and topology of the magnetic field, as well as the microwave feeding configuration. The dominance of the X-mode is also verified and plotted by using the power dissipation density distribution as a surface plot.

Acknowledgment

References

[1] Weatherford, B. R., "Development and Study of an Electron Cyclotron Resonance Waveguide Plasma Cathode for Electric Propulsion Applications," Ph.D. Thesis, The University of Michigan, Ann Arbor, MI, 2011.

[2] Hidaka, Y., Foster, J. E., Getty, W., Gilgenbach, R., and Lau, Y., "Performance and Analysis of an Electron Cyclotron Resonance Plasma Cathode," *Journal of Vacuum Science & Technology A*, Vol. 25, No. 4, 2007, pp. 781–790.

[3] Funaki, I., Kuninaka, H., and Toki, K., "Plasma Characterization of a 10-cm Diameter Microwave Discharge Ion Thruster," *Journal of Propulsion and Power*, Vol. 20, No. 4, 2004, pp. 718–727.

[4] Kamhawi, H., Foster, J. E., and Patterson, M. J., "Operation of a Microwave Electron Cyclotron Resonance Cathode," 40th *Joint Propulsion Conference*, Fort Lauderdale, FL, July 2004, AIAA 2004-3819.

[5] Herman, D. A., Soulas, G. C., and Patterson, M. J., "Status of the NEXT Ion Thruster Long-Duration Test After 10100 h and 207 kg Demonstrated," 43rd *Joint Propulsion Conference*, Cincinnati, OH, July 2007, AIAA 2007-5272.

[6] Funaki, I., Nishiyama, K., Kuninaka, H., Toki, K., Shimizu, Y., and Toki, H., "20mN-class Microwave Discharge Ion Thruster," 27th *International Electric Propulsion Conference*, Pasadena, CA, October 2001, IEPC 01-103.

[7] Kuninaka, H., Nishiyama, K., Funaki, I., Shimizu, Y., Yamada, T., and Kawaguchi, J., "Assessment of Plasma Interactions and Flight Status of the HAYABUSA Asteroid Explorer Propelled by Microwave Discharge Ion Engines," *IEEE Transactions on Plasma Science*, Vol. 34, No. 5, 2006, pp. 2125–2132.

[8] Nishiyama, K., Hosoda, S., Kuninaka, H., and Toyoda, Y., "Operational Characteristics of a Microwave Discharge Neutralizer for the ECR Ion Thruster μ20," 31st *International Electric Propulsion Conference*, Ann Arbor, MI, September 2009, IEPC 2009-21.

[9] Nishiyama, K., Kuninaka, H., and Nakai, T., "Two-Dimensional Characterization of Microwave E-fields and Beam Profiles of the ECR Ion Thruster μ20," 30th *International Electric Propulsion Conference*, Florence, Italy, September 2007, IEPC 2007-25.

[10] Lieberman, M. A. and Lichtenberg, A. J., *Principles of Plasma Discharges and Materials Processing*, New York, USA: John Wiley & Sons, 2005.

[11] Hagelaar, G., Makasheva, K., Garrigues, L., and Boeuf, J., "Modelling of a Dipolar Microwave Plasma Sustained by Electron Cyclotron Resonance," *Journal of Physics D: Applied Physics*, Vol. 42, No. 19, 2009, pp. 194019.

[12] Masui, H., Tashiro, Y., Yamamoto, N., Nakashima, H., and Funaki, I., "Analysis of Electron and Microwave Behavior in Microwave Discharge Neutralizer," *Transactions of the Japan Society for Aeronautical and Space Sciences*, Vol. 49, No. 164, 2006, pp. 87–93.